Catalysis Science & Technology

Accepted Manuscript

ROYAL SOCIETY OF CHEMISTRY

www.rsc.org/catalysis

Catalysis Science & Technology

ARTICLE

Simultaneous coking and dealumination of zeolite H-ZSM-5 during the transformation of chloromethane into olefins†

Received 00th January 20xx,
Accepted 00th January 20xx

DOI: 10.1039/x0xx00000x

www.rsc.org/

M. Ibáñez,[a] M. Gamero,[a] J. Ruiz-Martínez,[b] B.M. Weckhuysen,[b] A.T. Aguayo,[a] J. Bilbao,[a] P. Castaño*[a]

The deactivation pathways of a zeolite H-ZSM-5 catalyst, containing bentonite and α-Al_2O_3 as binder material, have been studied during the transformation of chloromethane into light olefins, which is considered as a possible step to valorize methane from natural gas. The reactions have been carried out in a fixed bed reactor, feeding pure chloromethane at 400, 425 and 450 °C; 1.5 bar and with a space-time of 5.4 ($g_{catalyst}$) h (mol_{CH2})$^{-1}$ during 255 min. The properties of the fresh and spent catalysts have been assessed by several techniques, such as N_2 physisorption, adsorption/desorption of NH_3, XPS and ^{29}Si NMR. Additional measurements of the spent catalysts have been performed to study the nature of the deactivating coke species: TG-TPO, SEM, FT-IR and UV-vis spectroscopies. With the results in hand, two deactivation mechanisms were proposed: irreversible dealumination at temperatures higher than 450 °C by HCl and reversible coke fouling, while coke formation results from the condensation of poly-alkylbenzenes, which are also intermediates for olefin production. The coke deposits grow in size with the addition of Cl to the carbonaceous structure.

1. Introduction

The increasing worldwide resources of natural gas, from conventional sources and non-conventional sources, such as shale gas, are spurring efforts to develop commercial processes to obtain fuels and chemicals from methane. The estimated reserves on methane in 2013 are 2.7 trillion cubic meters.[1] Additionally, methane also can be obtained in a sustainable manner from bacterial anaerobic digestion of waste streams (e.g. wastewater treatment plants).[2] Currently, methane is predominantly converted to synthesis gas and or hydrogen via catalytic steam reforming. One possible route to obtain fuels and chemicals from methane is the use of the synthesis gas for methanol, ethanol, butanol, dimethyl ether or Fischer-Tropsch synthesis routes.

Direct valorisation routes of methane in one stage processes, are less attractive for industrial implementation at large scale due to high pressure, high temperature, expensive catalyst or low selectivity and productivity with the current technology.[3-6]

Another conversion route, conceptually proposed by Mobil Oil,[7,8] is the oxyhydrochlorination of methane to obtain chloromethane, and the subsequent transformation of chloromethane to hydrocarbons at atmospheric pressure, moderated temperatures (< 450 °C) into hydrocarbons on a H-ZSM-5 zeolite catalyst. This last route generates great interest in order to avoid the energy demanding steam reforming step. The integration of these two stages in a process makes it more energetically efficient than methane gasification and the subsequent synthesis of methanol.

On the other hand, the second stage of chloromethane transformation involves similar reaction steps to those well-known in the methanol-to-hydrocarbons (MTH) or methanol-to-olefins (MTO) processes.[9,10] The lower reactivity of chloromethane with respect to methanol is related to its lower adsorption rate on Brønsted acid sites.[11] The chloromethane-to-hydrocarbons mechanism has been analyzed by FT-IR spectroscopy[12] and is believed to involve the following steps: (i) dissociation of chloromethane; (ii) formation of methoxy species on the acid sites; (iii) formation of poly-alkylbenzenes as active intermediates; (iv) olefins release, while parallel (v) hydrogen transfer and condensation reactions occur to form paraffins and aromatics. Other authors[13,14] observed that the steps (i) and (ii) are limiting the overall reaction and account for the longer induction period compared to the catalytic transformation of methanol in the MTH and MTO processes.

Several catalysts are active for the conversion of chloromethane into olefins. Among them, H-ZSM-5 and H-SAPO-34 are particularly promising. The rapid deactivation of H-SAPO-34 by coke limits the process lifetime, which is slightly attenuated by metals incorporation.[15-17] H-ZSM-5 shows less catalyst deactivation due to the higher diffusion rate of coke precursors and metal doping can enhance the zeolite catalyst performance.[18-22] The number of acid sites and the porous structure of zeolite H-ZSM-5 are the key parameters that influence the catalytic performance. The zeolite H-ZSM-5

Department of Chemical Engineering, University of the Basque Country (UPV/EHU). P.O. Box: 644, 48080. Bilbao (Spain)
Inorganic Chemistry and Catalysis group, Debye Institute for Nanomaterials Science, Faculty of Science, Utrecht University, Universiteitsweg 99, 3584 CG Utrecht (the Netherlands)

† Electronic Supplementary Information (ESI) available: [details of any supplementary information available should be included here]. See DOI: 10.1039/x0xx00000x

catalyst is the most suitable one taking into account the right compromise between conversion, propylene selectivity and stability.[23]

Catalyst deactivation hampers the implementation of the chloromethane-to-olefins process; therefore gaining fundamental understanding on this process is key to find solutions for the limited catalyst lifetime. This contribution aims to bring new understanding on the mechanisms of zeolite H-ZSM-5 catalyst deactivation during the transformation of chloromethane into olefins. Particularly, this work is focused on the study of coke deposition (i.e., reversible deactivation) and zeolite dealumination (i.e., irreversible deactivation), which are identified as the two main deactivation routes.[11,13,23,24] For this purpose, we have studied coke formation using different analytical techniques, namely TG-TPO, SEM, FT-IR and UV-Vis, while zeolite dealumination has been investigated by N_2 adsorption-desorption, NH_3-TPD, XPS and ^{29}Si NMR. Anticipating the dealumination of the zeolite, we have included Al in the composition of the matrix (binder and filler) for reducing the impact of this deactivation on the acid sites of the zeolite. The regenerability of the catalyst material has been studied by applying a series of reaction-regeneration cycles in other to determinate the reversibility conditions.

2. Experimental

2.1. Catalyst preparation

The commercial zeolite, supplied in its ammonium form by Zeolyst International (SiO_2/Al_2O_3 = 80), has been subjected to a calcination step (550 °C, 3 h) in order to remove the ammonia and obtain the acid form. Natural bentonite supplied by Exaloid and exchanged with NH_4NO_3 1 M (Panreac, 98 %) has been used as binder (30 wt%), and α-alumina (Prolabo, calcined at 1000 °C) as inert filler (45 wt%).

The catalyst particles have been obtained by wet extrusion, using a high-pressure hydraulic piston, through 0.8 mm diameter holes.[25] The extrudate materials obtained were dried: (i) at room temperature for 24 h, and (ii) later, in an oven at 110 °C for 24 h. Then the catalyst was sieved selecting a particle size between 0.15 and 0.3 mm. Finally the catalyst was calcined at 575 °C for 3 h. This temperature was reached following a ramp of 5 °C min^{-1}.

2.2. Reaction set-up and product analysis

The experiments were carried out by feeding chloromethane (AlphaGaz, 99.999 %) in an isothermal fixed bed reactor under the following operating conditions: 400 , 425 and 450 °C; 1.5 atm; and a space-time = 5.4 ($g_{catalyst}$) h (mol_{CH2})$^{-1}$. This low space-time was established to evaluate the deactivation more accurately, while the time on stream (TOS) = 255 min. For the analysis of the coke, different samples were obtained at 450 °C with time on stream (TOS) of: 5, 10, 15, 30, 45, 60, 75, 120 and 255 min.

The fixed bed reactor can operate up to 100 bar and 700 °C with a catalyst load of up to 5 g. The bed consists of a mixture of catalyst and inert solid, carborundum (CSi, supplied by Prolabo) in order to ensure an isothermal bed. The HCl formed during the reaction was removed by using two fixed bed adsorption reactors in series, made of a mixture of $CaCO_3$ (95 wt%) and Laponite (5 wt%). These materials were calcined at 800 °C thereby increasing the surface area and adsorption capacity. The gases from these catalytic beds pass through a particle filter of 5 µm mesh diameter and subsequently are cooled down to 170 °C. A fraction of the product stream is diluted in a He stream and continuously analyzed in a micro-chromatograph Varian CP-4900 GC. The remaining reaction stream is partially condensed in a Peltier cell at 0 °C and the uncondensed gas flow is vented.

2.3. Fresh and deactivated catalyst characterization

The physical or structural properties of the catalyst (i.e., BET surface area, micropore volume, pore volume, pore size distribution and pore diameter average) were measured using a Micromeritics ASAP 2010, these properties are determined by adsorption-desorption of N_2 (micropore and mesopore formation).

The acid properties of the catalyst materials were determined by NH_3 adsorption-desorption: the number of acid sites and average acid strength were obtained by monitoring the differential adsorption of NH_3 simultaneously by calorimetry and thermogravimetry in a Setaram TG-DSC 111 instrument and the curve for temperature programmed desorption of NH_3 has been obtained by connecting a Balzer Instruments mass spectrometer (Thermostar) on-line to a Setaram TG-DSC 111.[26,27]Before the NH_3adsorption,the catalyst sample has been pre-treated in He (160 mL min^{-1}) following a temperature ramp up to 550 ºC and kept in this temperature 1 h. The saturation of the sample is carried out at 150 ºC with 50 µL min^{-1} of ammonia. Then, the sample is kept in He flow to remove the physisorbed fraction of NH_3 for 1 h. The TPD was performed by heating the sample up to 550 ºC with a heating rate of 5 ºC min^{-1} in He (20 mL min^{-1}).

Scanning electron microscopy (SEM) images were performed with a JEOL JSM-6400 W filament (3.5 nm resolution), equipped with an X-Ray energy dispersive (EDX) analyzer Pentafet (Oxford, UK) up to 133 eV resolution.

The spectra of coupled polarized (CP) magic angle spinning (MAS) nuclear magnetic resonance (NMR) of ^{29}Si (^{29}Si CP-MAS NMR) were obtained using a Bruker 400 WB Plus spectrometer. Spectra were collected by using a 4 mm probe spinning at 10 kHz. The spectra of solid samples were recorded for 12 h using the standard pulse sequence, at 79.5 MHz, a spectral width of 55 kHz, a contact time of 2 ms and an inter pulse delay of 5 s. As the samples contain an alumina binder it was not possible to obtain reasonable results with ^{27}Al MAS NMR and therefore this approach has not been followed.

X-ray Photo-electron Spectroscopy (XPS) analysis has been carried out using a SPECS (Berlin, Germany) equipment with a Phoibos analyzer 150 1D-DLD and Al Kα (hν = 1486.6eV) monochromic radiation source. It has been first done on a wide range of elements present in the sample (wide scan: step

energy 1 eV, dwell time 0.1 s, pass energy 40 eV), while an exhausted analysis of elements (detail scan: step energy 0.1 eV, dwell time 0.1 s, pass energy 20 eV) was performed with an exit angle of electrons equal to 90°. The 1s carbon has been established at 284.6 eV to correct for possible charging effects. The XPS spectrometer has been previously calibrated with the peak of Ag $3d_{5/2}$ (368.28 eV). The XPS spectra were fitted using the software CasaXPS 2.3.16, which models the contributions Gaussian-Lorentzian, after background subtraction (Shirley).

2.4. Coke characterization

The amount of coke deposited on the catalyst was measured by combustion of a sample taken from the fixed bed reactor. Prior to the analysis, the sample was flown in 30 mL min^{-1} of He for 2 h to eliminate the volatiles that do not contribute to catalyst deactivation. The experiments were performed with a TGA Q5000TA thermobalance (Thermo Scientific) following the procedure: (1) scan of the sample with N_2 stream to remove impurities; (2) combustion with air at 575 °C with a temperature ramp of 3 °C min^{-1} followed by isothermal conditions for 60 min (to ensure complete combustion of coke); (3) the sample has been cooled with a ramp of 15 °C min^{-1} to 250 °C.

The chemical nature of the coke species was determined by ex-situ FT-IR spectroscopy by using a Nicolet 6700 spectrophotometer (Thermo). The deactivated catalyst sample (≈ 10 mg) was pressed into a self-supported pellet with KBr (150 mg, purity > 99%) applying a pressure equivalent to 10 t cm^{-2}. The sample was degassed in a transmission cell at 100 °C for 1 h to desorb water and remove the impurities of the sample.

The UV-Vis absorption measurements were carried out using a high-temperature UV-Vis probe provided by Avantes. The probe comprises one excitation and one collection optical fibber with a size diameter of 400 µm and length of 1.5 m, which are placed in a stainless steel protection sleeve. The probe was connected to a deuterium-halogen light soured and an AvaSpec 2048 UV-Vis spectrometer. The probe was custom-made to operate at temperatures up to 873 K. The samples were placed on a Scientific Instrument Linkam cell and spectra were collected at different positions along individual catalyst particles and in different catalyst particles, so that the results are averages of these measurements. The spectra were saved every 20 s, with 100 accumulations of 140 ms exposure time each. The optical absorption microscopic measurements were performed in the spectral range of 400–700 nm.

3. Results

3.1. Catalyst characterization

Table 1 summarizes the textural properties and number of acid sites of the catalyst material with binder as well as the pure zeolite H-ZSM-5 material used. The agglomeration of the zeolite contributes to the increasing mesopore volume from 0.15 cm^3 g^{-1} up to 0.47 cm^3 g^{-1}, and as a consequence, the pore diameter average increases up to 150 Å. On the other hand, the total number of acid sites decreases with 59 % (0.172 μmol_{NH3} g^{-1}) because the bentonite used to agglomerate has a low number of acid sites and the α-Al_2O_3 used as an inert binder material has insufficient acidy. The acid strength average decreases slightly with the agglomeration with a value of 116 kJ $(mol_{NH3})^{-1}$.

Table 1. Properties of the zeolite and the catalyst.

Property	Zeolite	Catalyst
BET surface area (m^2 g^{-1})	540	203
Micropore area (m^2 g^{-1})	396	106
Mesopore volume (cm^3 g^{-1})	0.154	0.468
Number of acid sites (µmol g^{-1})	0.427	0.172
Average acid strength (kJ $(mol)^{-1}$)	125	116

3.2. Coke deactivation

3.2.1. Kinetics of coke formation. Figure 1a displays the conversion of chloromethane with increasing time-on-stream (TOS) for the three selected reaction temperatures. In the same Figure 1a, the evolution of the coke content of the catalyst at 450 °C is represented. The evolution of the conversion of chloromethane with TOS (Figure 1a) shows the existence of three periods, in analogy with the methanol-to-olefins (MTO) process: (A) an initiation step where the conversion of chloromethane increases due to the incipient formation of poly-alkylbenzene reaction intermediates;[28,29] (B) a reaction step, in which the hydrocarbon pool is formed and the reaction most likely follows a dual mechanism with poly-alkylbenzenes and olefins as intermediates;[30] and (C) a deactivation step, where poly-aromatics compounds are formed during the condensation of inert poly-alkylbenzenes.[31] Each period has a different duration, which depends on the properties of the catalyst and reaction conditions as in the MTO process.[27-29] In this way, Figure 1a shows that the induction period is 35, 20 and 10 min at 400, 425 and 450 °C, respectively. In this period, chloromethane conversion increases to values above 80 wt% for the different reaction temperatures under study. On the reaction step (B), the formation of new active poly-alkylbenzenes species competes with the deactivation step (C) where aromatic condensates into larger structures that are inactive (coke).[31] An increase in the reaction temperature favours these condensation reactions and consequently the conversion drops and is negligible after 200 min at 450 °C.

Table S1 in supporting information summarizes the selectivity of products at different temperatures conditions studied here, at two time on stream for comparison. The explanation of the mentioned product distribution can be found in the supporting information too. Figure 1b shows the olefin selectivities at 15 min and 255 min for the different reaction temperatures and the coke content after 255 min TOS. The initial (15 min) olefin selectivity increases with

reaction temperature, but as the catalyst deactivates faster, the final (255 min) olefin selectivity decreases. These results also point out that the faster the formation of reaction intermediates (poly-alkylbenzenes) the faster the formation of light olefins, but also the faster the condensation reactions form coke deposits. When the coke content is higher than 3-4 wt%, the olefin selectivity is drastically affected.

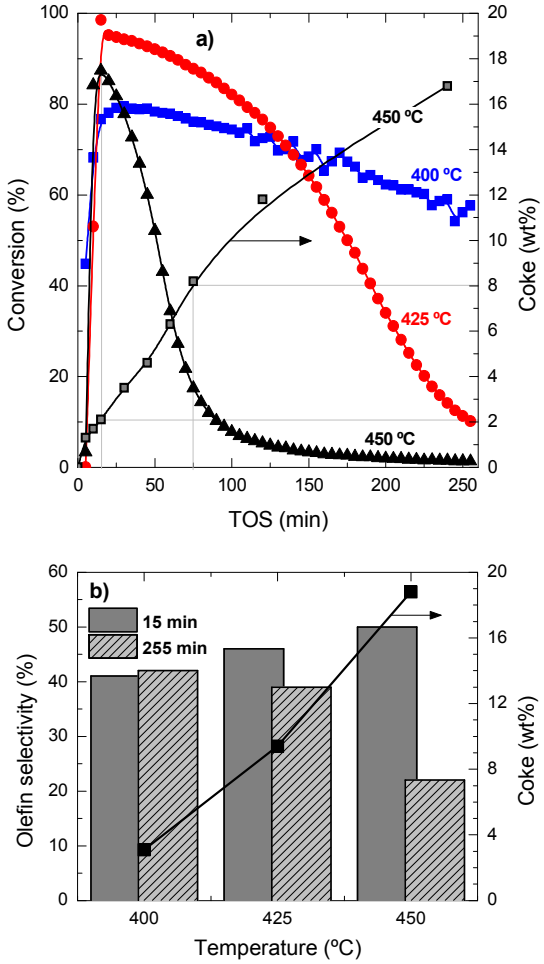

Figure 1. Evolution with time on stream of chloromethane conversion at different temperatures and coke content at 450 °C (a), and effect of temperature on the selectivity of light olefins at 15 and 255 min time on stream and the coke content at 255 min time on stream (b).

These results show that, in agreement with the methanol-to-olefin process, hydrocarbons trapped inside the porous structure of the catalyst material initially have a role as reaction intermediates and eventually condensate and block the acid sites and the micropores of the catalyst material. Accordingly, the deactivating coke is formed by the conversion of intermediate poly-alkylbenzenes to progressively inactive and more condensed structures.[31,32]

Figure 2 presents the TPO profiles of coke combustion deposited on the catalyst material at a reaction temperature of 450 °C for different TOS values. These profiles show the existence of two combustion peaks, associated with different composition and location of coke within the catalyst particles:[33,34] (i) coke I burns approximately at 430 °C and it has low condensation, poor graphitization and relatively high H:C ratio; (ii) coke II burns at 510 °C and it has a more condensed, higher graphitization and lower H:C ratio compared with coke I. Thus, the difference in the combustion maxima of these two types of coke could be associated, in principle, with both location and composition. Our previous results in other hydrocarbon conversion processes[33-36] suggest that the location and composition of the coke deposits are interconnected, as external coke has less steric hindrance to grow.[37] Interestingly, Figure 2 displays that the reaction temperatures at which the maximum combustion rate of coke I and II occur shifts to higher values at longer TOS values: (coke I) from 410 to 440 °C and (coke II) from 500 to 550 °C. This temperature shift indicates a higher degree of condensation of both types of coke with increasing TOS.

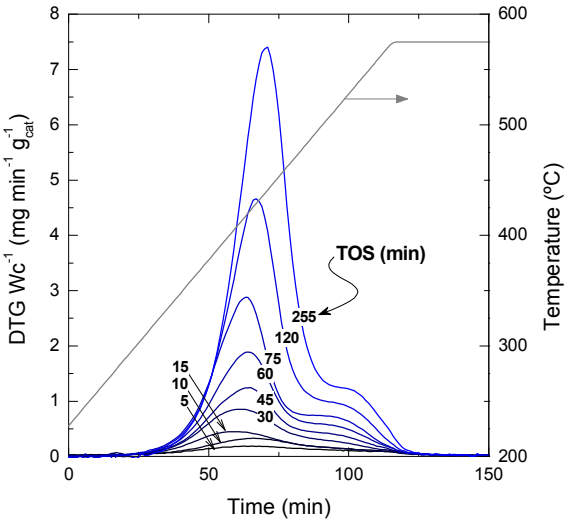

Figure 2. TPO profiles of the coke combustion deposited on the spent catalyst with different TOS, at 450 °C.

The quantification of the two different types of cokes has been performed by deconvolution of the TPO curves, assuming two independent first order kinetic models with respect to the partial pressure of O_2 (P_{O2}) and the fraction of coke content in the catalyst (C_{Ci}).[38] Figure 3a shows an example of the described deconvolution of the deactivated catalyst at 450 °C and at a TOS of 255 min. The shape of the second peak does not have a symmetrical Gaussian shape due to the fact that part of the combustion peak is obtained during the temperature ramp and the rest in an isothermal step, as shown in Figures 2 and 3a. Figure 3b displays the evolution of each coke fraction deposited at 450 °C with increasing TOS. During the first 75 min of reaction, which correspond to the initiation (A) and reaction period (B), the amount of coke I and II increases linearly and simultaneously, until the value of total

coke content of about 8 wt% (Figure 1), which corresponds to a coke I:II ratio of 1:1. At TOS higher than 75 min, in the deactivation period (C), coke I experiences continuous growth, while the coke II tends to an asymptotic value around 4.4 wt%. This difference in the evolution of the two types of coke can be explained by their different location on the porous structure of the catalyst. Thus, coke II is deposited in the pores of the catalyst material, so that the size of the zeolite H-ZSM-5 pores and/or these of the matrix limit its formation. Besides, coke II has lower H:C ratio and it is more condensed compared with coke I, reasons behind the higher combustion temperature of the former. In this process coke precursors are formed by the condensation of poly-alkylbenzenes and oligomerization of olefins.[14] Zeolite H-ZSM-5 has an ideal pore system, with high connectivity and without cages, enabling a fast circulation of coke precursors to the exterior of the zeolite material,[35,36,39,40] where these species grow without spatial constrain, forming coke I.[37] Given the negligible number of acid sites of bentonite and α-Al_2O_3, these binder materials have insignificant activity for these reactions of coke formation and thus, coke is mainly formed inside or outside the zeolite domains. All the steps of coke formation are favoured at higher reaction temperatures and with higher number of acid sites of the zeolite H-ZSM-5 employed.

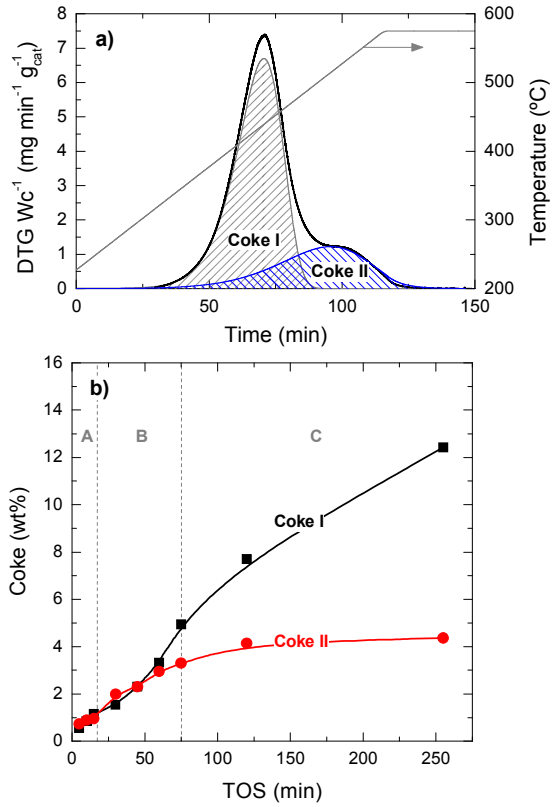

Figure 3. The two fractions of coke by deconvolution of TPO profile of spent catalyst at 255 min and 450 °C (a), and the evolution with time on stream of coke I and II (b).

3.2.2. The role of coke in catalyst deactivation. Figure 4 shows the evolution of the catalyst textural properties with the total coke content. The changes in the textural properties of the catalyst are dependent of the coke content and independent of the reaction temperature. The deterioration of the textural properties is faster during the initiation period (A) with a coke content of about 2 wt% than in the stationary periods (B) and deactivated (C). During the initiation period (A), coke I and II are already formed (Figure 3b) and there is a significant degradation of mesopores. The deterioration of the surface and pore volume is slower in the stationary period (B) and re-accelerates in the deactivation period (C) due to the (further) collapse of the catalyst porosity.

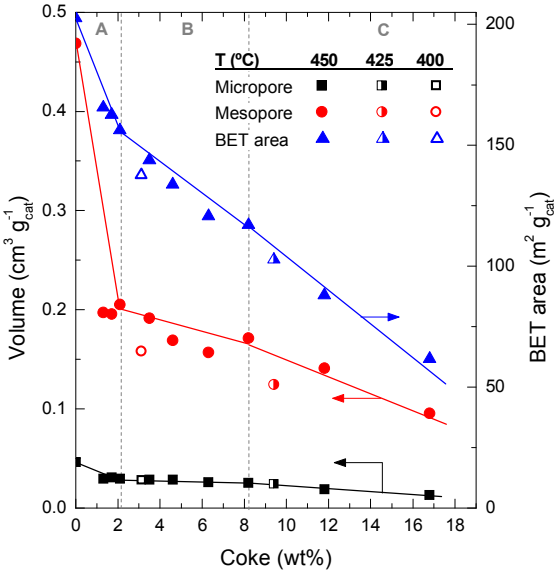

Figure 4. Evolution of coke content with the physical properties of the catalyst spent at different reaction temperatures.

Figure 5 shows the mesopore size distribution of the fresh and spent catalyst materials, which has been determined with the BJH method in the range of 3-100 nm. The results of Figure 5a correspond to different reaction temperatures but for the same TOS (i.e., 255 min), while Figure 5b corresponds to a reaction temperature of 450 °C but measured for different TOS values. It can be concluded that the fresh catalyst has a bimodal pore distribution with mesopores of 4 and 15 nm, presumably corresponding to the matrix of bentonite and α-Al_2O_3 and spaces between the zeolite H-ZSM-5 domains, which are formed during the agglomeration.[41] Furthermore, it appears that the 4 nm pores are plugged by coke deposits, whereas the 15 nm mesopores are narrowed down to 6 nm. Pore blockage is faster with increasing reaction temperature and TOS.

Figure 6 shows the degradation of the catalyst acid properties (i.e. total number of acid sites and average acid

strength) with coke content. These results also indicate a direct relationship between the remaining number of acid sites features and the coke content deposited on the catalyst material. The fresh catalyst has a number of acid sites of 172 µmol g_{cat}^{-1}, this value decreases to 126 µmol g_{cat}^{-1} after the A period, 79 µmol g_{cat}^{-1} after the B period and 62 µmol g_{cat}^{-1} after the C period. The rate of deterioration of the acid properties is much faster in the A period, but it reaccelerates in the C period. By comparing the drop of conversion (Figure 1a) with the catalyst number of acid sites (Figure 6) it can be concluded that the catalyst material has no activity for the conversion of chloromethane, but certain residual number of acid sites remains (< 80 µmol $gcat^{-1}$) with poor acid strength (< 80 kJ mol^{-1}). This residual number of acid sites is not sufficient to activate chloromethane and to convert its reaction intermediates into olefins. At this stage, the catalyst is active only for the reaction of coke with chloromethane. Thus, the coke content continues to increase with TOS in the period C (Figure 1), in particularly coke I (Figure 3b).

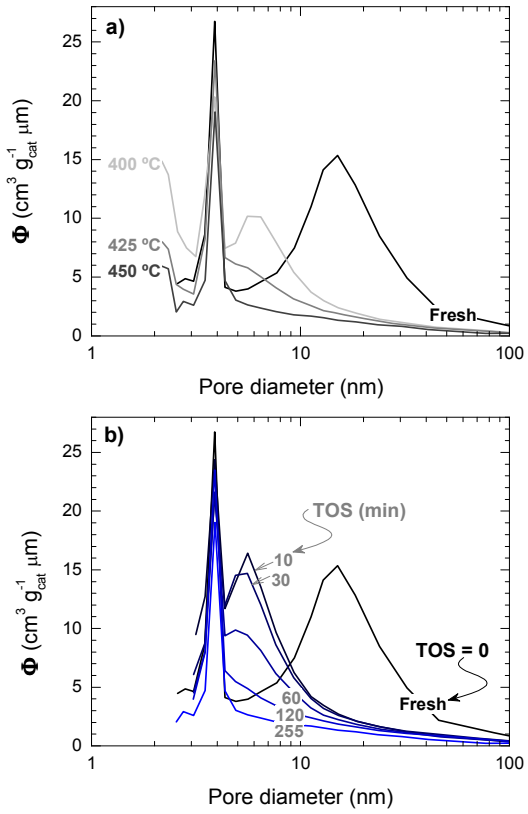

Figure 5. Coke deposition effect on the pore size distribution of the spent catalyst at different temperatures (TOS = 255 min) (a), and during different TOS (450 °C) (b).

3.2.3. Evolution of the coke composition during reaction. Different spectroscopic techniques were used to determine the coke composition and its evolution with increasing TOS. This analysis aids to understand the coke formation mechanism. The evolution of the normalized intensities of the FT-IR absorption bands is displayed in Figure 7. These IR bands correspond to different vibrational modes from the coke molecules deposited on the catalyst at different TOS. The IR band at 1425 cm^{-1} corresponds to stretching mode of C-Cl from -CH_2-Cl and aromatic-Cl groups.[16,42] The IR bands at 1580 cm^{-1} and 1610 cm^{-1} are ascribed to stretching mode of C=C bonds in poly-aromatic hydrocarbons (PAH) or in coke (dienes).[43] The C-H stretching band at 2930 cm^{-1} is most likely due to aliphatic -CH_2 and –CH groups, and the C-H stretching band at 2960 cm^{-1} to -CH_3 aliphatic groups. The band at 1425 cm^{-1} has no unique assignment, but considering its higher intensity respect to the same analysis used for the methanol-to-olefin process, part of it can be assigned to C-Cl bonds or chlorinated species in coke, whose intensity increases with TOS (Figure 7). The FT-IR results show that the IR bands of PAH, dienes and the one at 1425 cm^{-1} increase almost linearly during the A and B periods, whereas the IR bands of aliphatic groups and the one at 1425 cm^{-1} undergo a slight increase in the C period. These results indicate a growth of aromatic and olefinic species in coke, and an increasing growth of chlorinated and aliphatic species in the C period. The relative ratio of the IR intensities of -CH_3 and -CH_2 groups is almost constant, indicating that there is no significant variation in the length of the aliphatic chains in coke with increasing TOS.

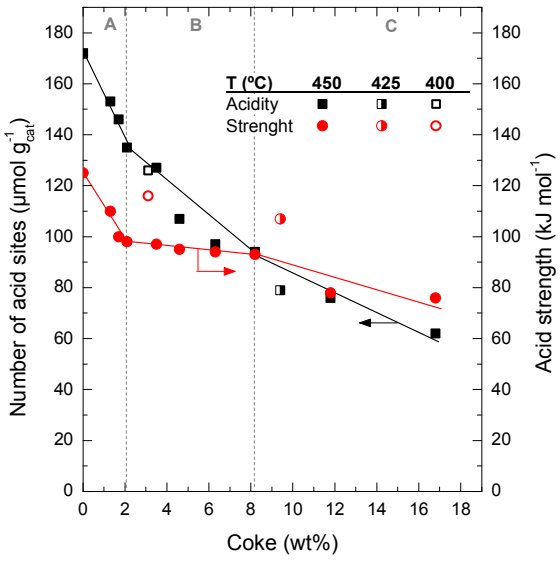

Figure 6. Evolution of coke content with the total number of acid sites and acid strength of the spent catalyst at different reaction temperatures and different TOS (450 °C).

UV-Vis absorption spectroscopy is sensitive to the electronic transitions of different aromatic species and it is a suitable technique for the analysis of the formation and growth of coke in different reactions, such as cracking of poly-olefins,[35,36] bio-oil cracking,[34,44] aromatization of paraffins and olefins,[45] dehydrogenation of paraffins,[46,47] as well as the MTO

reaction.[48] The region of UV-Vis absorption spectra between 300-410 nm has been assigned to π-π* transition originating from poly-alkylbenzenes carbocations (i.e., one ring aromatics) forming the "hydrocarbon pool",[49] at 425-475 nm more condensed aromatic compounds are observed, such as two and three ring aromatic carbocations from naphthalene, anthracene and phenanthrene,[45,50] more condensed species are observed at 565-635 nm, such as aromatic carbocation species with four and five rings,[33] and above 675-680 nm, higher condensation PAH carbocation structures appears.[33]

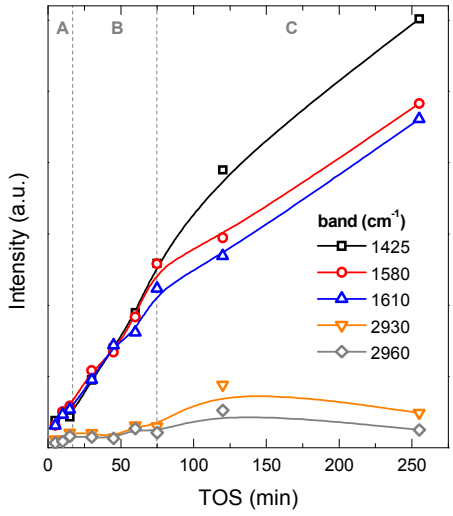

Figure 7. Evolution of the intensities of the FT-IR spectrum vibration bands with time on stream corresponding to functional groups of coke on the spent catalyst at 450 °C.

Figure 8 displays the changes of the intensities of the different absorption bands with increasing TOS obtained upon deconvolution of the UV-Vis spectra (Figure S2 of the supporting information shows these spectra) by using Gaussians. It is observed that the absorption bands at 380, 430, 480, 530 and 580 nm follow a first order kinetic formation, with an average formation time of 2-3 min, and the intensity of these absorption bands tending to an asymptotic value. The more condensed coke species, with absorption bands at 630, 680 and 730 nm (more evident in the last one) have a formation and growth stages similar to the ones observed to coke formation: (A period) in the range 0-30 min, with first order kinetic formation, (B period) 30-75 min with steady formation of these species and (C period) with accelerated growth of these bands. It is important to mention that the formation kinetics in the A period are very similar among the UV-Vis bands, however and after this period, less condensed one and two ring aromatics seem to reach a plateau of formation due to the fact that this type of active/inactive species lay inside the micropores of the zeolite H-ZSM-5 (with pores of 0.5-0.6 nm). In the B period but particularly in the C period, there is an incremental growth rate of the most condensed structures with probable participation of the chloromethane reactant.

The results showed so far demonstrate that the mechanisms of coke formation and further growth on a zeolite H-ZSM-5 catalyst is very similar for both MTO and chloromethane-to-olefins.[51] However, the rates of coke formation are considerably faster during the transformation of chloromethane into olefins. On the other hand, chloromethane is less reactive than methanol and the formation of poly-alkylbenzenes (initiation period A) is slower. The presence of steam during the methanol transformation has been found to be effective in reducing the condensation of coke precursors and to facilitate desorption of the acid sites of zeolite H-ZSM-5, in obtaining olefins from methanol[51] and other oxygenated compounds.[44,52] As steam is not created during chloromethane transformation this facilitation is not observed and, instead, HCl is present in the reaction media, which certainly will affect the overall stability of the catalyst material.

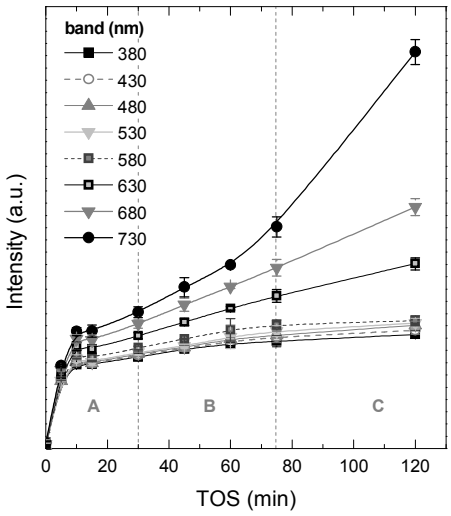

Figure 8. Evolution of the UV-Vis vibrations band intensities with time on stream corresponding to the aromatic species of coke on the used catalyst to 450 °C range.

3.3. Dealumination deactivation

While catalyst deactivation by coke formation is a reversible process and the catalyst can be regenerated by (gentle) coke combustion, the possible dealumination by HCl is irreversible.[53] To quantify the extent of this irreversible deactivation, the loss of catalyst activity has been studied in successive reaction-regeneration cycles using a space-time of 3.22 g_{cat} h $(mol_{CH2})^{-1}$, for 70 min of reaction and at 400, 425 and 450 °C. The regeneration step was performed by coke combustion with air in the reactor at 550 °C for 120 min.

Figure 9 shows the evolution with increasing TOS in a cycle of reaction-regeneration-reaction of the different products: methane, C_2-C_4 light olefins, non-aromatic C_{5+} hydrocarbons (C_{5+} HC), C_2-C_4 light paraffins and BTX aromatics. During reaction at 400 °C (Figure 9a), the regenerated catalyst recovers completely the initial catalytic performance so all the deactivation appears to be reversible. In contrast, when the reaction is performed at 450 °C (Figure 9b), the conversion and product yields do not follow the same performance in both reaction cycles and a less active catalyst is obtained in the second cycle.

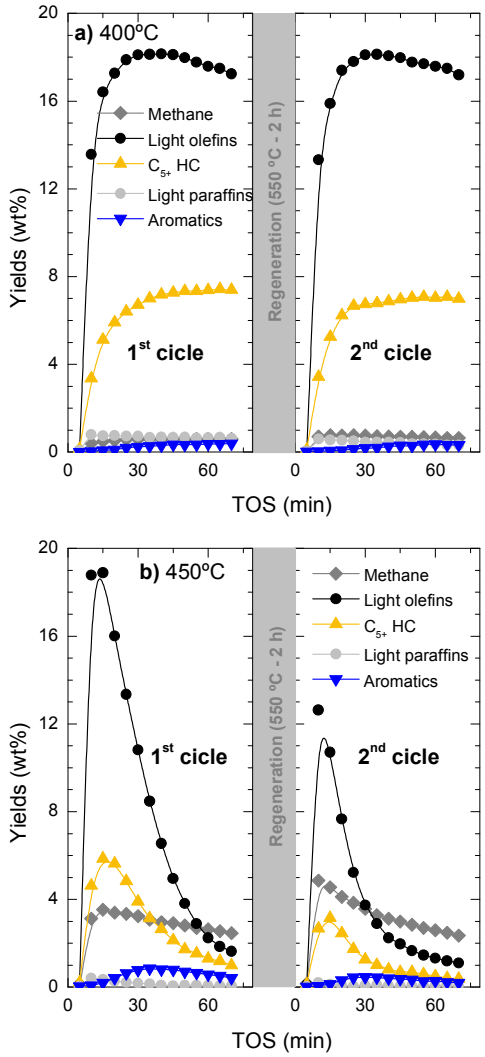

Figure 9. Evolution with time on stream of distribution products for the fresh catalyst (first cycle) at 400 °C (a) and 450 °C (b), and the yields using the same regeneration temperatures of catalyst (second cycle) by coke combustion at 550 °C for 2 h.

The results of Figure 9 indicate the presence of irreversible deactivation in the reaction step that favours parallel reactions like the competitive thermal cracking of chloromethane into methane. The irreversible loss of catalyst activity is unlikely to be attributed to the regeneration step due to the fact that the catalyst tested at 400 °C do not show any significant irreversible deactivation. The irreversible dealumination of the catalyst was studied using different analytical techniques, namely SEM-EDX, XPS and ^{29}Si NMR.

Figure 10a shows a SEM image of the deactivated catalyst, which has been reacting at 450 °C for 4 h, whereas Figure 10b shows the EDX spectra of the spots 1 and 2 in Figure 10a. The signals of Si, Al and O are present in the zeolite material and the matrix components, but a higher intensity of the Si indicates the higher proportion of H-ZSM-5 zeolite in the spot due to its higher fraction of SiO_2 (*ca*. 98 wt% accounting $SiO_2/Al_2O_3 = 80$) compared with that of bentonite (<70 wt%).[54,55] On the contrary, a higher proportion of Al indicates the higher proportion of the matrix material due to the fact that the filler is α-Al_2O_3. The signals of Mg and Fe univocally correspond to the bentonite matrix material.

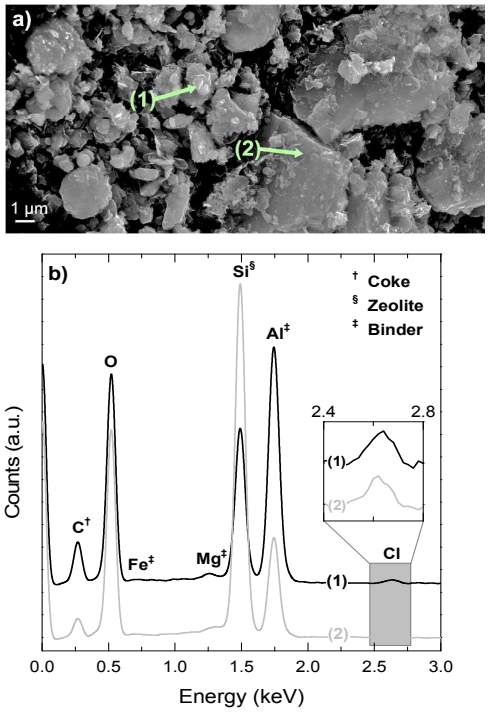

Figure 10. SEM image of the deactivated catalyst at 450 °C and 255 min of time on stream (a) and EDX analysis (b) in positions where there is a higher presence of the matrix material (point 1) and area richer in HZSM-5 zeolite material(point 2).

The results of Figure 10b demonstrate that position 1 has a higher proportion of the matrix components (higher signals of Al, Fe and Mg), whereas position 2 corresponds to an area richer in H-ZSM-5 zeolite material (higher signal of Si). On the other hand, the results of Figure 10b show that coke (C signal) is deposited mainly on the matrix material (point 1) in what we have referred as external coke, although, there is also a remarkable coke content on or inside the zeolite material. Figure 10b shows that the signal of Cl is present in positions 1 and 2 (that has been zoomed in for better visualization), which

means that the Cl is fixed in the catalyst in two ways: (i) with Al, $AlCl_3$ is most probably formed, and; (ii) in the organic phase of the deactivated catalyst, and therefore in the coke deposits, which is consistent with the presence of chlorinated groups aforementioned in the FT-IR spectra of the coke deposits. The mechanism of $AlCl_3$ formation has been observed in different zeolite materials exposed to HCl.[56-58] The high content of α-Al_2O_3 in the matrix suggests that this component protects (at least to some degree) the H-ZSM-5 zeolite material from dealumination.

Figure 11 shows the ^{29}Si NMR spectra of the fresh and spent catalyst materials treated at 400, 425 and 450 °C. The fresh catalyst shows a chemical shift at -118.18 ppm corresponding to several contributions (Q_4 of Si-$(OSi)_4$ to ca. -119 ppm, Q_4 of Si-$(OSi)_3(OAl)_1$ to ca. -117.5 ppm and Q_3 of Si-$(OSi)_3(OH)_1$ to ca. -116 ppm) in the zeolite material. In addition, other minor chemical shifts are observed at -112 and -102 ppm are attributable to Q_3 contributions in the bentonite.[59,60]The displacement of the maximum of the NMR peak from -118.61 to -119.11 ppm as the reaction temperature increases in the range 400-450 °C indicates a decrease of the Si-$(OSi)_3(OAl)_1$ contribution with respect to the Si-$(OSi)_4$ one. This result highlights the structural modification of the zeolite by dealumination. Indeed, this kind of dealumination of zeolite H-ZSM-5 has been observed in the transformation of different oxygenates (i.e., methanol, ethanol and bio-oil) to hydrocarbons, which is attributed to steaming at high reaction temperatures.[61-63] Based on the results obtained in the catalytic performance and the characterization of the spent catalysts, we can conclude that there is a significant dealumination of zeolite H-ZSM-5 at 450 °C due to the presence of HCl in the reaction media. This deactivation also leads to the formation of $AlCl_3$, which is consistent with the presence of Cl on the catalyst surface, as determined by EDX spectroscopy (Figure 10b).

To quantify the dealumination of the catalyst, the fresh and deactivated catalyst materials were evaluated by X-ray Photo-electron spectroscopy (XPS). The results of the Si/Al ratio are summarized in Table 2, using the bands of Si-2*p* (102.42 eV) and Al-2*p* (74.25 eV).[64] Note that these Si/Al ratios correspond to the Si and Al present in both the zeolite and the catalyst matrix. The Si/Al ratio of the spent catalyst at 400 °C is similar (i.e., 1.04) to that of fresh one (i.e., 1.06), while the value of the ratio increases notably for 425 °C (i.e., 1.23) but particularly at 450 °C (i.e., 1.60). All the above indicates that there is a significant dealumination of the catalyst material taking place at 450 °C. Presumably, the presence of extra aluminium in the matrix is beneficial for the quenching the irreversible dealumination of zeolite H-ZSM-5, diverting HCl into less harmful reactions (i.e., formation of $AlCl_3$ by reacting with the aluminium). Clearly, 425 °C is the upper reaction temperature to avoid irreversible catalyst deactivation by dealumination.

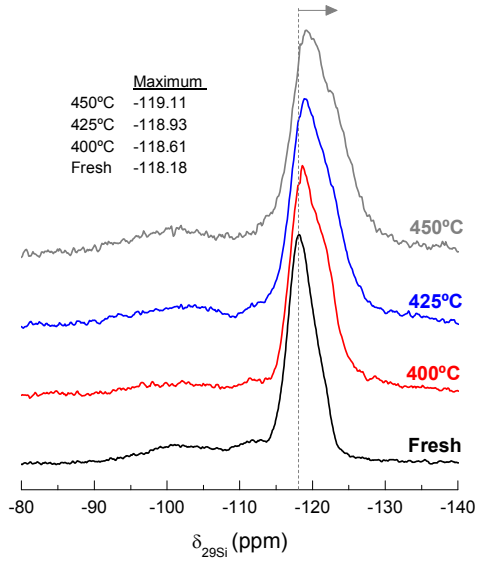

Figure 11. Effect of reaction temperature in the peak position of ^{29}Si NMR spectra; -118.18 ppm, of the fresh and used catalyst during 255 min time on stream.

Table 2. Areas of the bands corresponding to SiO_2 and Al_2O_3 obtained by deconvolution of the XPS spectra at specified binding energies (BE) and the ratio SiO_2/Al_2O_3 for the fresh and used catalyst at different temperatures.

Elements		BE (eV)	Area (%)			
			Fresh	400 °C	425 °C	450 °C
SiO_2	Si 2p	102.42	12.61	13.13	11.49	10.09
Al_2O_3	Al 2p	74.25	12.1	12.88	9.32	6.31
			SiO_2/Al_2O_3			
			1.04	1.02	1.23	1.6

Conclusions

In the catalytic transformation of chloromethane into olefins, the main cause of deactivation of zeolite H-ZSM-5 zeolite catalyst, containing bentonite and α-Al_2O_3 as binder material, is coke deposition (i.e., reversible deactivation) and the dealumination (i.e., irreversible deactivation) of the catalyst meanly at temperatures higher than 425 °C.

The mechanism of coke formation can be related to the three successive stages: Stage A, which is an initiation stage (until reach a coke content on the catalyst of about 2 wt%), associated with the incipient formation of active poly-alkylbenzenes in the micropores of the zeolite and simultaneous formation of inactive condensed aromatic structures in the mesopores and macropores (due to the deposition of the polyalkylbenzenes formed on the acid sites of the zeolite on the catalytic matrix); State B, which is a

reaction period (up to a coke content of about 8 wt%) with the fastest formation of olefins and reaction period of condensed coke structures, and; Stage C, which corresponds to complete deactivation observed by the apparent shutdown of olefin production, due to a remarkable blockage of the zeolite pores, deterioration of its number of acid sites and growth of condensed PAH structures.

The TPO combustion profiles show the existence two types of coke: Coke I is more hydrogenated (burns at 430 °C), less condensed and grows almost linearly with TOS; Coke II is less hydrogenated (burns at 510 °C), more condensed, has an asymptotic growth and reaches a saturating value. After 255 min of reaction at 450 ºC, the amount of coke I is almost 3 times as much as that of coke II (Figure 3). In this condition, the amount of coke deposited on the matrix material is higher than that on the zeolite material according the EDX results (Figure 10). Thus and accounting our previous works in other processes using H-ZSM-5 zeolite,[37,65] we inferred that coke I is mainly deposited on the matrix pores, outside the zeolite and with significantly less steric hindrance against its growth, whereas coke II is closer to the acid sites of the H-ZSM-5 zeolite material. The fact that the amount of coke I increases linearly even when the catalyst activity has shutdown (e.g. after 255 min at 450 ºC) indicate that the growth of this type of coke is due to the condensation with chloromethane, as the concentration of the rest of products is practically negligible.

Coke deactivation is reversible after carrying out the reaction at 400 °C and the catalyst material recovers completely its activity by coke combustion of with air at 550 °C for 2 h. However, performing the reaction at 425 °C or particularly at 450 °C, the catalyst is also deactivated irreversibly, without recovering completely the activity after combustion of coke. The results of the spectroscopic analysis have revealed that the dealumination of the zeolite material, which causes an increase of the relative abundance of species Si-$(OSi)_4$, and an increase of Si/Al ratio, can be attributed to the formation of $AlCl_3$ by reaction of the HCl released during catalytic reaction. Consequently, it is necessary to perform the chloromethane-to-olefins reaction at a reaction temperature of 400 °C or lower in order to recover fully the activity of the material upon regeneration.

Acknowledgements

The financial support of this work was undertaken by the Ministry of Science and Education of the Spanish Government (Project CTQ2010-19188, Project CTQ2010-19623, CTQ2013-46172-P and CTQ2013-46173-R), of the Basque Government (Project IT748-13 and Project BFI-2012-203), M.G is grateful for the postgraduate grant from the University of the Basque Country (No. UPV/EHU2013), the University of the Basque Country (UFI 11/39 UPV/EHU) and the Dutch Government (CW-NWO (TOP and VENI grants)).

References

1. M. Melikoglu, *Renewable and Sustainable Energy Reviews*, 2014, **37**, 460-468.
2. L. Yang, X. Ge, C. Wan, F. Yu and Y. Li, *Renewable and Sustainable Energy Reviews*, 2014, **40**, 1133-1152.
3. J. H. Lunsford, *Catalysis Today*, 2000, **63**, 165-174.
4. J. S. Ahari, R. Ahmadi, H. Mikami, K. Inazu, S. Zarrinpashne, S. Suzuki and K. i. Aika, *Catalysis Today*, 2009, **145**, 45-54.
5. A. Holmen, *Catalysis Today*, 2009, **142**, 2-8.
6. A. G. Dedov, G. D. Nipan, A. S. Loktev, A. A. Tyunyaev, V. A. Ketsko, K. V. Parkhomenko and I. I. Moiseev, *Applied Catalysis A: General*, 2011, **406**, 1-12.
7. C. D. Chang, in *Studies in Surface Science and Catalysis*, 1988, pp. 127-143.
8. C. E. Taylor, R. P. Noceti and R. R. Schehl, in *Stud. Surf. Sci. Catal.*, 1988, pp. 483-489.
9. N. Rahimi and R. Karimzadeh, *Applied Catalysis A: General*, 2011, **398**, 1-17.
10. Y. K. Park, C. W. Lee, N. Y. Kang, W. C. Choi, S. Choi, S. H. Oh and D. S. Park, *Catalysis Surveys from Asia*, 2010, **14**, 75-84.
11. M. H. Nilsen, S. Svelle, S. Aravinthan and U. Olsbye, *Appl. Catal. A: Gen.*, 2009, **367**, 23-31.
12. T. Xu, Q. Zhang, H. Song and Y. Wang, *J. Catal.*, 2012, **295**, 232-241.
13. S. Svelle, S. Aravinthan, M. Bjørgen, K. P. Lillerud, S. Kolboe, I. M. Dahl and U. Olsbye, *J. Catal.*, 2006, **241**, 243-254.
14. U. Olsbye, O. V. Saure, N. B. Muddada, S. Bordiga, C. Lamberti, M. H. Nilsen, K. P. Lillerud and S. Svelle, *Catal. Today*, 2011, **171**, 211-220.
15. Y. Wei, D. Zhang, L. Xu, Z. Liu and B. L. Su, *Catalysis Today*, 2005, **106**, 84-89.
16. Y. Wei, D. Zhang, Z. Liu and B. L. Su, *Journal of Catalysis*, 2006, **238**, 46-57.
17. Y. Wei, Y. He, D. Zhang, L. Xu, S. Meng, Z. Liu and B. L. Su, *Microporous and Mesoporous Materials*, 2006, **90**, 188-197.
18. P. Lersch and F. Bandermann, *Appl. Catal.*, 1991, **75**, 133-152.
19. Y. Sun, S. M. Campbell, J. H. Lunsford, G. E. Lewis, D. Palke and L. M. Tau, *J. Catal.*, 1993, **143**, 32-44.
20. D. Jaumain and B. L. Su, *Catalysis Today*, 2002, **73**, 187-196.
21. D. Jaumain and B. L. Su, *Journal of Molecular Catalysis A: Chemical*, 2003, **197**, 263-273.
22. L. A. Noronha, E. F. Souza-Aguiar and C. J. A. Mota, *Catal. Today*, 2005, **101**, 9-13.
23. Y. Xu, J. Wang, Y. Suzuki and Z. G. Zhang, *Catalysis Today*, 2012, **185**, 41-46.
24. Y. Wei, D. Zhang, L. Xu, F. Chang, Y. He, S. Meng, B. l. Su and Z. Liu, *Catalysis Today*, 2008, **131**, 262-269.
25. P. L. Benito, A. T. Aguayo, A. G. Gayubo and J. Bilbao, *Ind. Eng. Chem. Res.*, 1996, **35**, 2177-2182.
26. A. G. Gayubo, A. T. Aguayo, M. Olazar, R. Vivanco and J. Bilbao, *Chemical Engineering Science*, 2003, **58**, 5239-5249.
27. A. T. Aguayo, A. G. Gayubo, R. Vivanco, M. Olazar and J. Bilbao, *Appl. Catal. A: Gen.*, 2005, **283**, 197-207.
28. A. T. Aguayo, A. G. Gayubo, R. Vivanco, A. Alonso and J. Bilbao, *Ind. Eng. Chem. Res.*, 2005, **44**, 7279-7286.
29. A. G. Gayubo, A. T. Aguayo, A. Alonso and J. Bilbao, *Ind. Eng. Chem. Res.*, 2007, **46**, 1981-1989.
30. M. Bjørgen, S. Svelle, F. Joensen, J. Nerlov, S. Kolboe, F. Bonino, L. Palumbo, S. Bordiga and U. Olsbye, *Journal of Catalysis*, 2007, **249**, 195-207.
31. Y. Jiang, J. Huang, V. R. Reddy Marthala, Y. S. Ooi, J. Weitkamp and M. Hunger, *Microporous and Mesoporous Materials*, 2007, **105**, 132-139.

32. M. Guisnet and P. Magnoux, *Appl. Catal. A: Gen.*, 2001, **212**, 83-96.
33. P. Castano, G. Elordi, M. Ibanez, M. Olazar and J. Bilbao, *Catalysis Science & Technology*, 2012, **2**, 504-508.
34. M. Ibanez, B. Valle, J. Bilbao, A. G. Gayubo and P. Castano, *Catalysis Today*, 2012, **195**, 106-113.
35. P. Castaño, G. Elordi, M. Olazar, A. T. Aguayo, B. Pawelec and J. Bilbao, *Appl. Catal. B: Environ.*, 2011, **104**, 91-100.
36. G. Elordi, M. Olazar, G. Lopez, P. Castaño and J. Bilbao, *Appl. Catal. B: Environ.*, 2011, **102**, 224-231.
37. E. Epelde, M. Ibañez, A. T. Aguayo, A. G. Gayubo, J. Bilbao and P. Castaño, *Microporous Mesoporous Mater.*, 2014, **195**, 284-293.
38. A. G. Gayubo, B. Valle, A. T. Aguayo, M. Olazar and J. Bilbao, *Energy Fuels*, 2009, **23**, 4129-4136.
39. L. Pinard, S. Hamieh, C. Canaff, F. Ferreira Madeira, I. Batonneau-Gener, S. Maury, O. Delpoux, K. Ben Tayeb, Y. Pouilloux and H. Vezin, *Journal of Catalysis*, 2013, **299**, 284-297.
40. M. Guisnet and P. Magnoux, *Appl. Catal.*, 1989, **54**, 1-27.
41. P. Castaño, J. Ruiz-Martinez, E. Epelde, A. G. Gayubo and B. M. Weckhuysen, *ChemCatChem*, 2013, **5**, 2827–2831.
42. P. B. E. Pretsch, M. Badertscher, *Structure Determination of Organic Compounds*, Springer, Berlin, 2009.
43. N. Arsenova, H. Bludau, W. O. Haag and H. G. Karge, *Microporous Mesoporous Mater.*, 1998, **23**, 1-10.
44. B. Valle, P. Castaño, M. Olazar, J. Bilbao and A. G. Gayubo, *Journal of Catalysis*, 2012, **285**, 304-314.
45. Y. M. Chung, D. Mores and B. M. Weckhuysen, *Appl. Catal. A: Gen.*, 2011, **404**, 12-20.
46. A. Iglesias-Juez, A. M. Beale, K. Maaijen, T. C. Weng, P. Glatzel and B. M. Weckhuysen, *Journal of Catalysis*, 2010, **276**, 268-279.
47. M. J. Wulfers, G. Tzolova-Muller, J. I. Villegas, D. Y. Murzin and F. C. Jentoft, *J. Catal.*, 2012, **296**, 132-142.
48. E. Borodina, F. Meirer, I. Lezcano-González, M. Mokhtar, A. M. Asiri, S. A. Al-Thabaiti, S. N. Basahel, J. Ruiz-Martinez and B. M. Weckhuysen, *ACS Catalysis*, 2015, **5**, 992-1003.
49. D. Mores, J. Kornatowski, U. Olsbye and B. M. Weckhuysen, *Chemistry - A European Journal*, 2011, **17**, 2874-2884.
50. P. Castaño, A. Gutiérrez, I. Hita, J. M. Arandes, A. T. Aguayo and J. Bilbao, *Energy and Fuels*, 2012, **26**, 1509-1519.
51. A. T. Aguayo, P. Castaño, D. Mier, A. G. Gayubo, M. Olazar and J. Bilbao, *Industrial and Engineering Chemistry Research*, 2011, **50**, 9980-9988.
52. A. G. Gayubo, A. Alonso, B. Valle, A. T. Aguayo, M. Olazar and J. Bilbao, *Fuel*, 2010, **89**, 3365-3372.
53. M. D. Argyle and C. H. Bartholomew, *Catalysts*, 2015, **5**, 145-269.
54. S. Catarino, M. Madeira, F. Monteiro, F. Rocha, A. S. Curvelo-Garcia and R. B. de Sousa, *J. Agric. Food Chem.*, 2008, **56**, 158-165.
55. R. Eriksson and T. Schatz, *Appl. Clay Sci.*, 2015, **108**, 12-18.
56. I. Batonneau-gener, A. Yonli, S. Hazael-pascal, J. Pedro Marques, J. Madeira Lopes, M. Guisnet, F. Ramoa Ribeiro and S. Mignard, *Microporous Mesoporous Mater.*, 2008, **110**, 480-487.
57. M. D. Gonzalez, Y. Cesteros and P. Salagre, *Microporous Mesoporous Mater.*, 2011, **144**, 162-170.
58. J. P. Marques, I. Gener, P. Ayrault, J. C. Bordado, J. M. Lopes, F. R. Ribeiro and M. Guisnet, *Microporous and Mesoporous Materials*, 2003, **60**, 251-262.
59. C. Breen, J. Madejová and P. Komadel, *Appl. Clay Sci.*, 1995, **10**, 219-230.
60. J. G. Thompson, *Clay Miner.*, 1984, **19**, 229-236.
61. D. Ma, Y. Lu, L. Su, Z. Xu, Z. Tian, Y. Xu, L. Lin and X. Bao, *J. Phys. Chem. B*, 2002, **106**, 8524-8530.
62. S. M. Maier, A. Jentys and J. A. Lercher, *J. Phys. Chem. C*, 2011, **115**, 8005-8013.
63. L. H. Ong, M. Dömök, R. Olindo, A. C. Van Veen and J. A. Lercher, *Microporous and Mesoporous Materials*, 2012, **164**, 9-20.
64. C. D. Wagner, W. M. Riggs, L. E. Davis and J. F. Moulder, *Handbook of X-Ray Photoelectron Spectroscopy*, Perkin-Elmer Corporation, Minnesota, 1979.
65. M. Ibáñez, M. Artetxe, G. Lopez, G. Elordi, J. Bilbao, M. Olazar and P. Castaño, *Appl. Catal. B: Environ.*, 2014, **148–149**, 436-445.